Acetone Adsorption on Ice Surfaces in the Temperature Range $T = 190-220$ K: Evidence for Aging Effects Due to Crystallographic Changes of the Adsorption Sites

P. Behr, A. Terziyski, and R. Zellner*

Institute of Physical and Theoretical Chemistry, University of Duisburg-Essen, D-45117 Essen, Germany

Received: November 4, 2005; In Final Form: April 25, 2006

The rate and thermodynamics of the adsorption of acetone on ice surfaces have been studied in the temperature range $T = 190-220$ K using a coated-wall flow tube reactor (CWFT) coupled with QMS detection. Ice films of 75 ± 25 μm thickness were prepared by coating the reactor using a calibrated flow of water vapor. The rate coefficients for adsorption and desorption as well as adsorption isotherms have been derived from temporal profiles of the gas phase concentration at the exit of the flow reactor together with a kinetic model that has recently been developed in our group to simulate reversible adsorption in CWFTs (Behr, P.; Terziyski, A.; Zellner, R. *Z. Phys. Chem.* **2004**, *218*, 1307−1327). It is found that acetone adsorption is entirely reversible; the adsorption capacity, however, depends on temperature and decreases with the age of the ice film. The aging effect is most pronounced at low acetone gas-phase concentrations ($\leq 2.0 \times 10^{11}$ molecules/cm^3) and at low temperatures. Under these conditions, acetone is initially adsorbed with a high rate and high surface coverage that, upon aging, both become lower. This effect is explained by the existence of initially two adsorption sites (1) and (2), which differ in nature and number density and for which the relative fractions change with time. Using two-site dynamic modeling, the rate coefficients for adsorption (k_{ads}) and desorption (k_{des}) as well as the Langmuir constant (K_L) and the maximum number of adsorption sites ($c_{s,max}$), as obtained for the adsorption of acetone on sites of types (1) and (2) in the respective temperature range, are $k_{ads}(1) = 3.8 \times 10^{-14}\ T^{0.5}$ cm^3 s^{-1}, $k_{des}(1) = 4.0 \times 10^{11} \exp(-5773/T)$ s^{-1}, $K_L\ (1) = 6.3 \times 10^{-25} \exp(5893/T)$ cm^3, $c_{s,max}(1) \leq 10^{14}$ cm^{-2} and $k_{ads}(2) = 2.9 \times 10^{-15}\ T^{0.5}$ cm^3 s^{-1}, $k_{des}(2) = 1.5 \times 10^7 \exp(-3488/T)$ s^{-1}, $K_L(2) = 5.0 \times 10^{-22} \exp(3849/T)$ cm^3, $c_{s,max}(2) = 6.0 \times 10^{14}$ cm^{-2}, respectively. On the basis of these results, the adsorption of acetone on aged ice occurs exclusively on sites of type (2). Among the possible explanations for the time-dependent two-site adsorption behavior, i.e., crystallographic differences, molecular or engraved microstructures, or a mixture of the two, we tentatively accept the former, i.e., that the two adsorption sites correspond to cubic (1, I_c) and hexagonal (2, I_h) sites. The temporal change of I_c to I_h and, hence, the time constants of aging are consistent with independent information in the literature on these phase changes.

1. Introduction

Studies of the interaction of atmospheric trace gases with surfaces have become an important subject of atmospheric chemistry ever since the discovery of larger regional atmospheric changes, such as the springtime Antarctic ozone hole[2−5] or the tropospheric ozone depletion in the Artic.[6−8] The characteristics of each of these events is the rapid change of gas-phase chemical composition due to the adsorption and chemical reaction of halogen- and/or nitrogen-containing trace gases with the surfaces of liquid or solid particles leading to the release of so-called activated trace gases, which upon submission to solar radiation are transferred into ozone-depleting free radicals.[9]

The rates of heterogeneous reactions in the atmosphere are generally expressed by a collision number with the available surface area multiplied by a reactive uptake coefficient, γ. The latter is a composite of all individual processes that are sequentially encountered in a heterogeneous reaction, i.e., adsorption, thermal equilibration, desorption, surface reaction, phase boundary transition, and bulk reaction.[10−13] The separation of the individual elementary processes, notably the rate of adsorption as expressed by a sticking or accommodation coefficient, of a reactive uptake process has only been possible in selective cases.[14−17] Moreover, the theoretical framework has just begun to be developed.[18,19]

An important part of heterogeneous interaction in the atmosphere apart from chemical reaction is the adsorption of trace gases on surfaces. In recent years, ice surfaces in the atmosphere have received considerable attention. The reason is that these surfaces may play an important role in some of the reactive trace gas modifications encountered in large-scale perturbations of atmospheric chemical composition. Ice surfaces occur among polar stratospheric clouds (PSCs) at temperatures below the lower stratospheric frost point,[20−22] in the form of cirrus clouds[23,24] as well as condensation trails (contrails) of jet aircraft,[25,26] both at temperatures in the regime 190−220 K as appropriate to the upper troposphere/lower stratosphere.[24] Moreover, ice surfaces are generated regularly during strong precipitation events of thunderstorms where rapid vertical motions of air masses lead to super cooling events and deposition freezing may become an important condensation process at high ice supersaturations.[27,28]

As a result of their importance, studies of chemical reactions and adsorption on ice surfaces have received substantial interest. This interest focuses on reactive uptake coefficients (see review by Abbatt, 2003[29]) as well as on the kinetics and thermodynam-

* To whom correspondence should be addressed. E-mail: reinhard.zellner@uni-essen.de.

10.1021/jp0563742 CCC: $33.50
Published on Web 06/10/2006

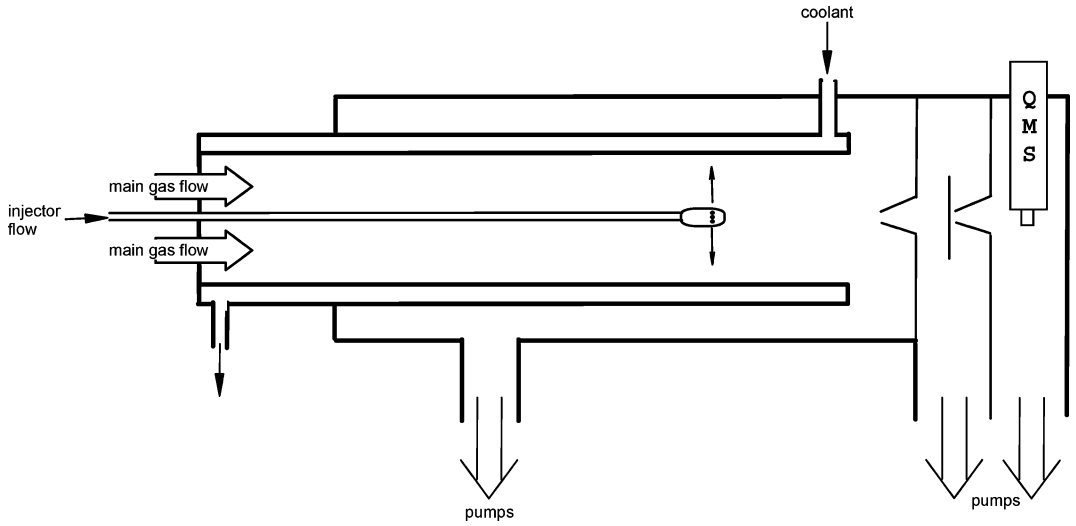

Figure 1. Schematic representation of differentially pumped coated-wall flow tube reactor with QMS detection.

ics of adsorption processes. The latter have recently been suggested to impact on oxygenated trace gases such as CH_2O, CH_3OH, C_2H_5OH, acetone, and others due to the expected strong interactions with ice surfaces at the low temperatures of the UTLS region and because of the occurrence of these compounds at surprisingly high concentrations in this part of the atmosphere.[30−32] Because such compounds are expected to impact on the concentration levels of the HO_x oxidation system,[33−36] investigations of their phase partitioning are important prerequisites of the assessment of their atmospheric chemical behaviors.

The aims of adsorption studies on surfaces focus on the thermodynamics of adsorption (adsorption enthalpies, fractional surface coverages) as well as on kinetic quantities such as adsorption and desorption rate constants. More recently, dynamical studies on surface collisions such as thermalization and energy dissipation[37,38] as well as dynamic residence time studies[16,39,40] have been added to the list of approaches to investigate surface/gas interactions. Needless to say that important contributions have also been provided by molecular configurational studies of adsorbate/surface structures using different levels of theory.[41,42]

Ice surfaces represent a special kind of surface due to their relatively high vapor pressures even at temperatures around 200 K. Under equilibrium conditions with the vapor phase, ice surfaces are extremely dynamic with simultaneous condensation and evaporation events. Under these conditions, ice surfaces have been found to be polycrystalline[43] with cubic (I_c) and hexagonal (I_h) ice being the most relevant structures. Both phases have very similar physical properties, i.e., density and interatomic distances.[44,45]

Adsorption studies on ice surfaces have frequently been performed in coated-wall flow tube reactors (CWFTs).[1,50−53] The advantage of this technique is that, in addition to adsorption equilibria, the exposure time can be varied and, hence, adsorption rate coefficients can also be determined. Moreover, the interaction of the gas phase with the surface can be kept kinetically controlled and is not diffusion limited, at least in the low-pressure operational mode.[35]

Adsorption measurements in flow reactors rely on the analysis of the gas-phase component at the downstream exit of the flow reactor. It has been found, though, in such studies[1,52,53] that temporal profiles of gas-phase components show complex shapes due to the interaction of adsorption and desorption processes. As a result, the derivation of thermodynamic and kinetic data is complicated and a theoretical framework is necessary to facilitate such analysis.[1,54] In the present paper, we present an application of this model to derive kinetic and thermodynamic data for the adsorption of acetone on ice under the effect of a changing adsorption capacity as a result of aging. To our knowledge, this effect has not been observed in acetone adsorption studies before.

2. Experimental Section

The adsorption of acetone on ice surfaces has been studied in a tubular flow reactor with the detection of acetone (sensitivity $\approx 10^{10}$ molecules cm^{-3}) using quadrupole mass spectrometry. The reactor consists of a jacketed flow tube of 24-mm internal diameter and 25-cm length that can be thermostated down to 180 K. Using a thermocouple, the temperature inside the reactor was measured with an accuracy of ± 1 K. The injection of acetone is through a sliding injector of 6-mm outer diameter. A schematic representation of the experimental setup is shown in Figure 1. The measurements were performed with typical pressures in the flow tube of $\sim$3 mbar and linear flow velocities of $\sim$1.5 ms^{-1} using He as a carrier gas. Model simulations for uptake kinetics in CWFT reactors indicate that the uptake is not limited by diffusion in the gas phase at typical uptake coefficients of about $\gamma \approx 0.01$[1].

Surface ice films were generated by the deposition of gaseous water upon injection of water vapor through the sliding injector at temperatures of the reactor wall of around 200 K; the ice film temperature was subsequently adjusted to that required in the experiment. During coating, the injector is slowly moved to generate an approximately uniform surface film. From the amount of water deposited, it is estimated that the surface film generated is approximately 50−100 microns thick, which corresponds formally to approximately 40 000 monolayers. It must be pointed out, however, that the concept of monolayers may not be meaningful due to the expected morphological roughness of the surface,[46] which also causes the total available surface area to exceed the geometric surface area (vide infra). As will be discussed below, water condensation at temperatures around 200 K generates a mixture of two different adsorption sites.

During normal uptake studies, additional water has not been added through the injector. It needs to be noted, though, that due to the high dynamics of ice surfaces at temperatures around and—more effectively—above 200 K, continuous desorption

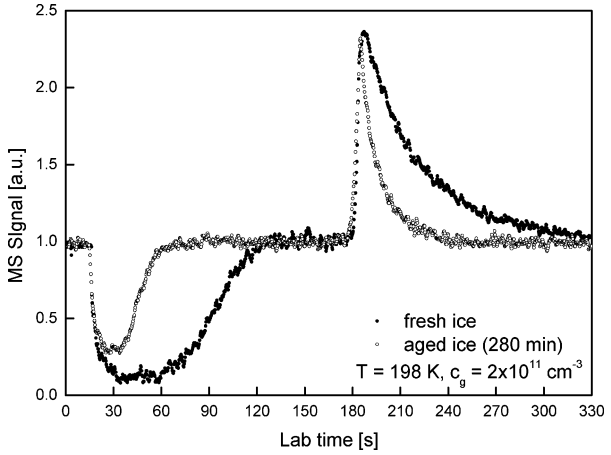

Figure 2. Adsorption and desorption profiles for acetone on ice at $T = 198$ K and $c_{gas} = 2 \times 10^{11}$ molecules/cm^3 as obtained by moving the injector sequentially in upstream and downstream directions. The two profiles are for different ages of the ice surface and correspond to a total number of adsorbed molecules of 7.3×10^{13} and 2.4×10^{13} cm^{-2}, respectively.

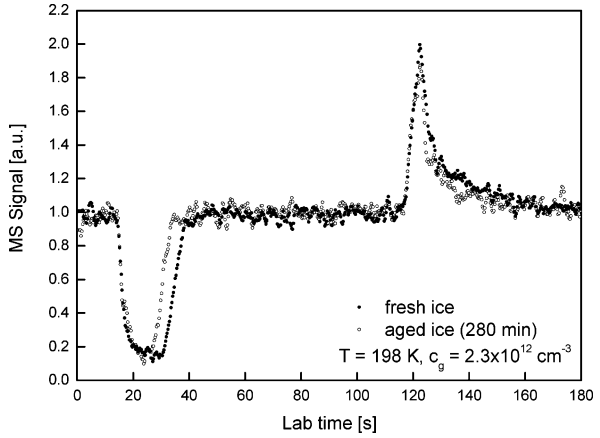

Figure 3. Same as for Figure 2 but for an acetone concentration of 1.6×10^{13} molecules/cm^3. The change of the adsorption capacity due to aging amounts to approximately 5×10^{13} cm^{-2}.

(evaporation) of water molecules from the surface will occur[47,55,56] and will lead to a thinning of the surface film. However, a more quantitative assessment of this effect leads to the conclusion that this film thinning will only occur at the very upstream end of the coated surface. Further downstream, the water vapor will be re-adsorbed. In fact, it can be shown from simple desorption/adsorption modeling that for the most part of the total length of the flow reactor, the surface ice film is in equilibrium with its corresponding vapor pressure and that a net loss of water vapor only occurs at the expense of the most upstream fraction of the surface layer. Additional water vapor needs not be introduced into the flow reactor to compensate for losses by pumping.[1] All adsorption measurements are hence being performed in the presence of equilibrium water vapor. Whether or not the dynamics of the water surface is accompanied by a temporal reduction of the film roughness, and hence of the total available surface area, is not known. On the other hand, there is little reason to expect that this should be the case because the morphology of the surface should be invariable for isothermal conditions at reversible equilibrium and under net adsorption flux as during coating.

3. Results

The kinetics and thermodynamics of the interaction of acetone with ice surfaces in the temperature range $T = 190-220$ K have been investigated by measurements of the temporal profiles of gaseous acetone as a result of increasing and decreasing, respectively, exposure of acetone to the surface ice film. This has been achieved by moving the injector in either upstream or downstream direction, in which case adsorption and desorption can be observed sequentially. To measure adsorption isotherms, the acetone concentration has been varied between 2.5×10^{10} and 1.0×10^{14} molecules/cm^3 at different temperatures.

3.1. Adsorption/Desorption Behavior and Aging Effects. A typical sequence of adsorption and desorption profiles for the interaction of acetone with an ice surface at lower temperatures, i.e., $T = 198$ K, and lower acetone concentrations, i.e., $\sim 2 \times 10^{11}$ molecules/cm^3 , is shown in Figure 2. As can be seen, adsorption and desorption profiles have different shapes that result from the response of the flow-tube walls on the gas-phase acetone concentration as a result of the change of the injector position. In fact, it can be shown that these differences in shapes are characteristic for reversible adsorption in CWFT reactors that permit the independent determination of adsorption and desorption rate constants[1]. The areas under the two parts of the profiles, however, are identical within experimental error, which implies that under these conditions, the adsorption of acetone is entirely reversible. We have no evidence for a permanent loss of acetone to the surface under all conditions encountered in our experiments.

Figure 2 also exemplifies the differences that we observe for an ice surface that is freshly prepared and one that has been aged for several hours. Although the principal behavior for adsorption and desorption is identical in each case, the areas under the respective adsorption/desorption profiles are considerably smaller for an aged ice surface. As a consequence, we note a reduction of the adsorption capacity as a result of aging under isothermal conditions. Because the total surface areas for adsorption and desorption are found to be invariant with time, aging does not seem to effect the reversibility of the uptake.

The amount of acetone adsorbed is increasing with the gas-phase concentration. To investigate how these variables influences the aging behavior, we have performed similar experiments at the same temperature but at higher acetone concentrations. As can be seen in Figure 3, the resulting adsorption/desorption profiles are substantially larger in size but exhibit equally an aging effect, albeit apparently less pronounced because the relative change of adsorption capacity is found to be smaller. However, when the change of areas is converted into absolute numbers of adsorbed molecules, the resulting change of net adsorption capacity (i.e $\sim 5 \times 10^{13}$ cm^{-2}) is nearly identical to that observed for lower acetone concentrations.

As will be shown below, both experiments have been performed under submonolayer adsorption and, hence, Langmuir conditions. The effect of isothermal aging is then suggested to be related to a change of the nature of surface sites from initially type (1) to—finally—type (2). Because each of these have their individual properties with respect to the rate and thermodynamics of adsorption (vide infra), aging is relatively less pronounced at higher adsorptions. It should be noted, though, that, in agreement with a two site adsorption model and a substantial reduction of adsorption capacity with increasing temperature, aging is not observed at higher temperatures.

The isothermal aging effect observed in our experiments at lower temperatures occurs on the time scale of hours. To investigate this kinetics in more detail, we have performed a series of experiments in which we have systematically varied the relative laboratory time (RLT) between successive adsorption/desorption profiles at $T = 198$ K. In each case, we have

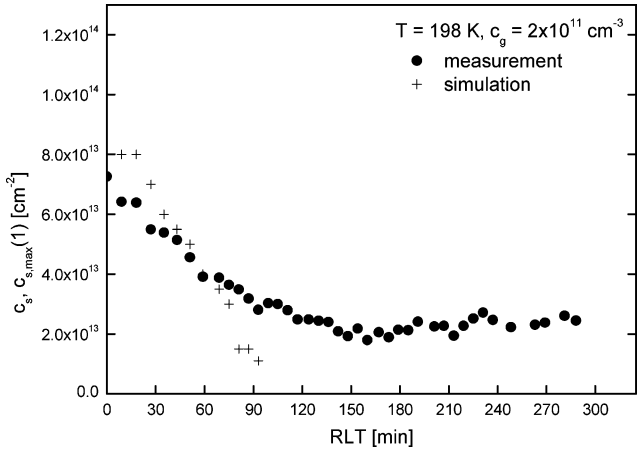

Figure 4. Temporal variation of the adsorption capacity (no. of molecules of acetone adsorbed per cm^2) of ice as a function of the age of the ice surface as expressed by the relative laboratory time (RLT). $T = 198$ K, $c_g = 2.0 \times 10^{11}$ cm^{-3}. Comparison of measured (•) and simulated data (+) using a two-adsorption site model (see text).

measured the resulting adsorption capacity, i.e., the number of acetone molecules adsorbed. The resulting variation of this capacity as a function of relative laboratory time is shown in Figure 4.

As can be seen from these experiments, this capacity decreases with a time constant of ~50 min, and hence an aging rate constant of ~0.02 min^{-1}, at $T = 198$ K. After complete aging, roughly 2/3 of the initial capacity is lost. Included also in Figure 4 is the result from a simulation study for the temporal change of the maximum number of adsorption sites of type (1) using a dynamic two-site model. The parameters used to describe this change are $k_{ads}(1) = 5.4 \times 10^{-13}$ cm^3 s^{-1}, $k_{ads}(2) = 3.0 \times 10^{-14}$ cm^3 s^{-1}, $k_{des}(1) = 0.31$ s^{-1}, $k_{des}(2) = 0.1$ s^{-1}, $c_{s,max}(1)$ = up to 1.0×10^{14} cm^{-2} (depending on RLT), and $c_{s,max}(2) = 6.0 \times 10^{14} cm^{-2}$.

A systematic variation of the aging rate constant with temperature has as of yet not been performed. As mentioned above, however, preliminary results indicate that aging is less pronounced at higher temperatures and not observable at all above 220 K. In more quantitative terms, the aging rate coefficient is found to have an activation energy on the order of 48 kJ/mol, whereupon aging at temperatures above 220 K may easily escape our observation. This is because our experiments cannot be performed much faster than over the time scale of several minutes. It should also be noted that we have experienced some influence on the aging effect caused by the thickness of the ice film, which indicates that aging is not exclusively a surface effect but is also somewhat influenced by the bulk of the ice phase.[57]

3.2. Adsorption Isotherms. One of the major objectives of the present work was to measure adsorption isotherms to extract the enthalpy of interaction and to predict the amount of acetone adsorbed on ice surfaces for different temperature conditions. As a consequence, we have tempted to cover an as wide as possible range of temperature. However, it became soon apparent that, due to the magnitude of the interaction enthalpy between ice and acetone, the accessible temperature range for reversible adsorption was rather limited. Moreover, the effect of aging has also been noted in adsorption isotherm measurements and due care had to be taken—at least at low temperatures—to measure adsorbed amounts of acetone at comparable ages of the ice surfaces.

Figure 5 shows the measured adsorption isotherm at $T = 193$ K for a range of acetone concentrations of less than 2.3×10^{12} molecules/cm^3 and for different ages of the ice surface. As can be seen, the data show an enormous scatter if they are taken as measured and if the age of the ice surface is left unconsidered. Only upon sorting of the overall data into different age "bins" do single Langmuir curves become apparent from which Langmuir constants (K_L) and maximum coverages ($c_{s,max}$) could be extracted (vide infra).

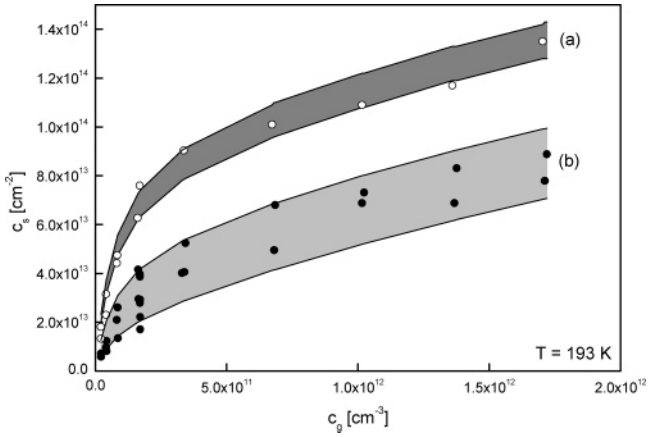

Figure 5. Langmuir plot for acetone adsorption on ice surfaces at $T = 193$ K and low ($\leq 2 \times 10^{12}$ cm^{-3}) acetone gas-phase concentrations. The data encompassed by the different curves are for (a) a fresh ice surface (~30 min) and (b) an aged ice surface (~220 min). Within each of the shaded areas, $c_{s,max}(1)$ changes from 9.5×10^{13} to 8.0×10^{13} cm^{-2} in case (a) and from 5.0×10^{13} to 2.0×10^{13} cm^{-2} in case (b).

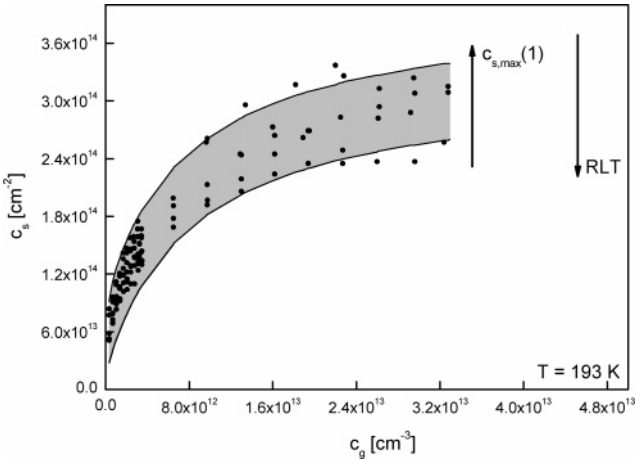

Figure 6. Same as Figure 5 but for an extended scale of the concentrations. The data shown are obtained for ages of the ice surface between 5 and 300 min. The upper and lower boundaries of the shaded area correspond to $c_{s,max}(1) = 10 \times 10^{13}$and 2×10^{13} cm^{-2}, respectively. In each case, $c_{s,max}(2) = 3 \times 10^{14}$ cm^{-2}.

As much as for the areas of the adsorption/desorption profiles, the effect of higher acetone concentrations on aging is also noticeable for the adsorption isotherm. An extension of the data of Figure 5 to acetone concentrations of up to 3.2×10^{13} molecules/cm^3 is shown in Figure 6. The most important point to notice here is that although the aged isotherm is almost at saturation with $c_{s,max}$ in the order of 2.5×10^{14} molecules/cm^3 for the highest acetone gas-phase concentration applied, the amount of acetone adsorbed for a young ice surface is still increasing at this concentration, implying a still larger $c_{s,max}$ value. The curves representing the upper and lower boundaries of the isotherms have been obtained from a two-site dynamic model in which the maximum number of adsorption sites for type (1) ice changes from 10×10^{13} to $2 \times 10^{13} cm^{-2}$ over the

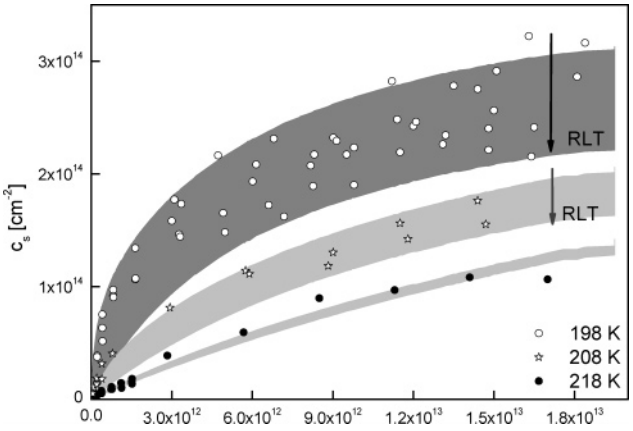

Figure 7. Adsorption isotherms for acetone on ice surfaces for temperatures of 198, 208, and 218 K. The upper and lower boundaries of the isotherms at 198 and 208 K reflect fresh (0−5 min) and aged (300 min) ice surfaces, respectively (see text).

time interval 5−300 min, whereas the corresponding number for type (2) sites is left time invariant at 3×10^{14} cm^{-2}.

As opposed to the adsorption isotherms measured at low temperatures those measured at higher temperatures show a much weaker aging effects. This is shown in Figure 7, where we present adsorption isotherms for 198, 208, and 218 K. All the data presented have been taken at ages of the ice surface between 10 and 250 min. As opposed to the data at 198 K for which there is still substantial aging, the effect is becoming smaller at 208 K and is no longer noticeable for 218 K. The upper boundaries for the isotherms at 198 and 208 K correspond to initial maximum numbers of adsorption sites of type (1) of 9×10^{1} and 4×10^{13} cm^{-2}, respectively. For the lower boundaries, this number has been set to zero in each case, corresponding to complete conversion of type (1) into type (2) sites after aging.

3.3. Adsorption at Two Different Surface Sites and Its Dynamics. To account for the aging effect observed and to extract adsorption parameters according to Langmuir theory, we have used a two-site dynamic adsorption model. In this model, the total adsorption of acetone onto an ice film is supposed to be governed by two different adsorption sites corresponding to type (1) and type (2) ice, respectively. Each of these types have their individual Langmuir parameters K_L and $c_{s,max}$ as well as their individual adsorption and desorption kinetics. The effect of aging, and hence the loss of adsorption capacity, is then attributed to a change of type (1) into the more stable type (2) form.

The Adsorption Model. The rates of surface coverage under conditions of reversible adsorption to each of the two different adsorption sites are given by the following equations:

$$\frac{dc_{s(1)}}{dt} = k_{ads(1)}c_g(c_{s,max(1)} - c_{s(1)}) - k_{des(1)}c_s$$

and

$$\frac{dc_{s(2)}}{dt} = k_{ads(2)}c_g(c_{s,max(2)} - c_{s(2)}) - k_{des(2)}c_s$$

where c_s and $c_{s,max}$ are the surface concentrations of acetone and their maximum values, respectively, in molecules/cm^2 and c_g is the gas-phase concentration of acetone in molecules/cm^3. The rate coefficient for adsorption k_{ads} (in units of cm^{-3} s^{-1}) is given by the simple gas kinetic expression $k_{ads} = \gamma_{ads}\sigma_0(1/4)\sqrt{(8RT/\pi M)}$, where γ_{ads} is the uptake coefficient and σ_0 is the collisional cross section for adsorption (in units of cm^2). The product $\gamma_{ads}\sigma_0$ is assumed to be temperature independent so that the temperature dependence of k_{ads} is simply given by the temperature dependence of the average gas-phase molecular velocity ($T^{1/2}$). The rate coefficient for desorption k_{des} (in units of s^{-1}), on the other hand, is given by a simple Arrhenius expression $k_{des} = A \times \exp(-E_a/RT)$ where E_a is approximately equal to the enthalpy of adsorption (ΔH_{ads}). With these definitions, it is obvious that adsorption of acetone on two different surface sites is associated with different kinetics and thermodynamics which—as a result of aging—both change with time, at least at lower temperatures.

The total rate of adsorption as expressed by the overall rate of surface coverage is given by the sum of the two terms, i.e.,

$$\frac{dc_s}{dt} = \frac{dc_{s(1)}}{dt} + \frac{dc_{s(2)}}{dt}$$

The corresponding change of the gas-phase concentration c_g of acetone is related to this surface change by the relation

$$\frac{dc_g}{dt} = -\frac{2}{r}\frac{dc_s}{dt}$$

which is valid for tubular reactors. Because in our experiment only c_g (or its proportional MS signal) is monitored, the above equations and their integrals are being jointly used to extract the desired parameter, namely k_{ads}, k_{des}, and $c_{s,max}$ for each of the two adsorption sites. This is done by fitting of the calculated gas phase concentration as a function of laboratory time to the measured adsorption and desorption profiles. As will be shown below, of the above parameters, only $c_{s,max}(1)$ is concluded to change with time as a result of aging and, hence, of the conversion of type (1) to type (2) adsorption sites.

Thermodynamic and Kinetic Considerations. Adsorption/desorption profiles such as those presented in Figures 2 and 3 contain two different kinds of information. The obvious one is the size of the areas under the adsorption/desorption peaks that are related to the Langmuir constant K_L and/or the maximum number of surface sites $c_{s,max}$. These areas are expected to change with temperature according to the van t'Hoff equation $d \ln K_L/dT = -\Delta H_{ads}/RT$.

Moreover, changes of the overall adsorption capacity as a function of relative laboratory time, as observed during aging, are also related to these quantities. However, K_L and $c_{s,max}$ are independent parameters that are, in principle, not coupled. They can be derived from the shapes of the adsorption isotherms. Needless to say that for submonolayer coverage, $c_{s,max}$ can also be temperature dependent. However, from our measurements, we have no evidence that this is the case.

A second and perhaps more important information contained in adsorption and desorption profiles is the kinetics of the interaction process, i.e., k_{ads} and k_{des}. In fact, the shape of these profiles is fairly sensitively influenced by the magnitudes of these rate coefficients, whereas the areas are reflecting the number of adsorbed species and, hence, K_L and/or $c_{s,max}$. In Figure 8, we present a comparison of measured and simulated adsorption/desorption profiles as obtained from best fits. As can be seen, the agreement is very satisfactory both with respect to shape and total area. A more detailed test of the sensitivity of best-fit parameters on the quality of the fits is demonstrated in Figure 9a−c. In this figure, we present the results of simulations in which we have varied the independent variables k_{ads}, k_{des}, and $c_{s,max}$. Varying the adsorption rate coefficient by a factor

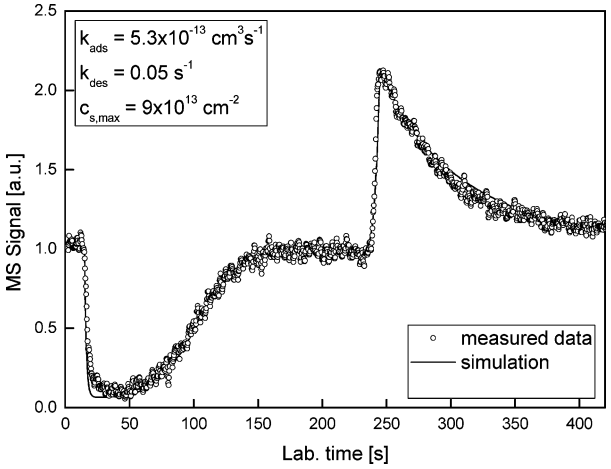

Figure 8. Comparison of measured and simulated adsorption/desorption profiles for the adsorption of acetone on fresh ice at $c_g = 1 \times 10^{11}$ cm^{-3} and $T = 193$ K. The resulting best-fit parameters for adsorption under these conditions, i.e., for the predominant existence of adsorption sites of type (1), are given in the insert of the figure.

of 2 in either direction (Figure 9a) strongly influences the rate of recovery—as expressed by the corresponding slopes—of the adsorption/desorption equilibrium. This is not the case for a variation of k_{des} (Figure 9b). In each case, however, the total areas change because, with the variations of k_{ads} and k_{des}, also the Langmuir constant is altered. Therefore, Figure 9c presents the result of simulations in which k_{ads} was varied but the total number of adsorbed species was kept constant by modifying $c_{s,max}$ in accord with the impact of k_{ads} on K_L. As a result again, the strong impact of k_{ads} on the slope of the recovery fraction of the adsorption profile is noted.

In summary, variations of the rate coefficients and $c_{s,max}$ by a factor of ± 2 are clearly distinguishable from the best-fit curves. Hence, we conclude that the absolute accuracy of our derived rate coefficients and $c_{s,max}$ is in the order of 50% for the analysis of one single measurement. Using more than a hundred measurements for one temperature and different initial gas-phase concentrations leads to an error of <20% in the values reported in Table 1. The sensitivities presented here and their derived accuracies are found not to change with the age of the ice surface.

The analysis of adsorption/desorption profiles using the a numerical fit of the corresponding rate equations are the key to the derivation of our kinetic and thermodynamic data. The results obtained from fitting a total of more than 100 adsorption/desorption vs laboratory time profiles are summarized in Table 1. As can be seen from this table, we have indeed succeeded to extract independent kinetic and thermodynamic data for the adsorption of acetone on ice films on two different active sites, which according to our interpretation correspond to cubic and hexagonal ice lattice structures (vide infra). The differences between the two are both in the kinetics of surface occupation as well as in the enthalpies of adsorption and the maximum number of sites available in each case.

According to our model, the kinetics of adsorption is determined by a second-order process between gas-phase molecules and unoccupied surface sites. The rate coefficient for this process is the gas kinetic collision number of these molecules with active surface sites of cross section $\sim 1 \times 10^{15}$ cm^2 [31] multiplied with a reactive uptake coefficient γ[1]. Because k_{ads} is on the order of 5×10^{-13} and 5×10^{-14} cm^{-3} s^{-1} for both type (1) and type (2) surface sites, respectively, the corresponding γ values differ by more than an order of magnitude in favor of type (1) ice (cf. Table 1).

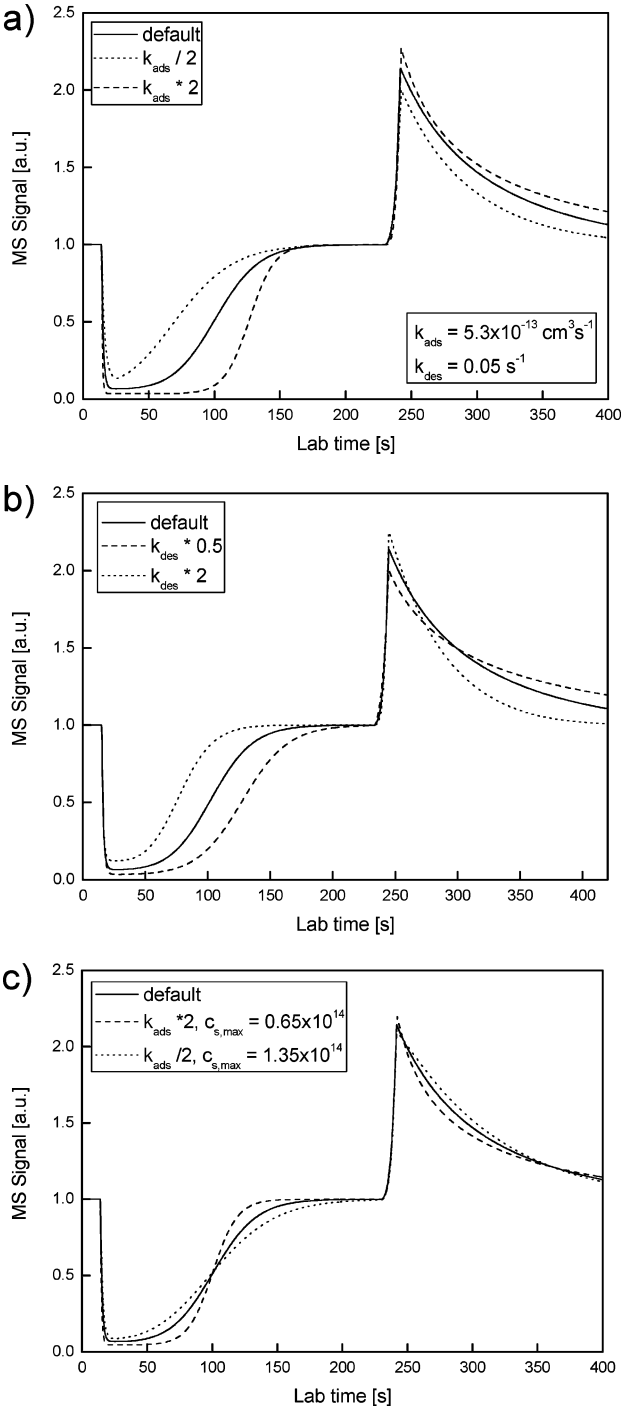

Figure 9. Sensitivity of adsorption/desorption peak profiles for acetone on ice surfaces on the rate coefficients k_{ads} and k_{des} as well as the maximum surface coverage $c_{s,max}$ at $T = 193$ K. The effects of varying k_{ads} and k_{des} individually are shown in (a) and (b), wheras in (c) we present the combined variation of k_{ads} and $c_{s,max}$. In each case, the bold curve represents the default fit of the experimental data of Figure 8.

A similar difference as for the adsorption rates also exists for the desorption rates. It is found that the desorption of acetone from type (1) sites has a pre-exponential factor of $\sim 4 \times 10^{11}$ s^{-1}, more than a factor of 10 larger than that of the type (2) sites ($A_{des} \approx 1 \times 10^{10}$ s^{-1}). In terms of transition state theory, this difference implies a "looser" transition state configuration or else a higher transmission factor associated with a higher frequency of vibration in the critical coordinate. The rate coefficient for desorption from the two different sites are presented graphically in Arrhenius form in Figure 10.

TABLE 1: Summary of Rate Coefficients and Adsorption Constants (K_L, $c_{S,Max}$) for the Interaction of Acetone (Adsorption, Desorption) with Ice Surfaces in the Temperature Range $T = 193-218$ K Differentiated for Sites (1) and (2) Corresponding to Cubic (I_c) and Hexagonal (I_h) Ice

	Type (1)/Cubic Ice		Type (2)/Hexagonal Ice	
T	k_{des} s^{-1}	k_{ads} 10^{-13} cm^3 s^{-1}	k_{des} s^{-1}	k_{ads} 10^{-14} cm^3 s^{-1}
193	0.04	5.30	–	–
198	0.09	5.37	0.31	4.03
203	0.18	5.44	0.55	4.08
208	0.39	5.50	0.64	4.13
213	0.67	5.57	1.08	4.18
218	-	–	1.66	4.22
γ	$(8 \pm 1)\ 10^{-2}$		$(6 \pm 1)\ 10^{-3}$	
	$E_{act,\ des}$ /kJ mol^{-1}		$E_{act,\ des}$/kJ mol^{-1}	
	48 ± 3		29 ± 6	

	Type (1)/Cubic Ice		Type (2)/Hexagonal Ice	
T	K_L 10^{-12} cm^3 (Th)[a]	K_L 10^{-12} cm^3 (Km)[b]	K_L 10^{-14} cm^3 (Th)[a]	K_L 10^{-14} cm^3 (Km)[b]
193	11.6	13.3	–	–
198	6.7	6.0	15.1	13.0
203	3.4	3.0	7.4	7.4
208	1.2	1.4	6.4	6.5
213	0.7	0.8	3.2	3.9
218	–	–	2.5	2.5
	E_{act}/kJ mol^{-1} (Th)		E_{act}/kJ mol^{-1} (Km)	
	49±3		32 ± 6	
	$c_{s,max}/cm^{-2}$		$c_{s,max}/cm^{-2}$	
	$\leq 1\ 10^{14}$		$6 \pm 1\ 10^{14}$	

[a] Th = thermodynamics. [b] Km = kinetic model.

The most interesting information of this plot is the difference in activation energies. Whereas the value for type (1) sites is on the order of 49 kJ/mol, the corresponding value for type (2) is only around 30 kJ/mol. If the reverse process of adsorption is assumed to occur without any barrier, as is indicated from our measurements of the temperature dependence of k_{ads}, then this difference is clearly a reflection of the enthalpies of adsorption, which is larger in the case of type (1) ice sites. This is shown in Figure 11 where we present the van t'Hoff plot of the Langmuir constants for each of the two adsorption sites.

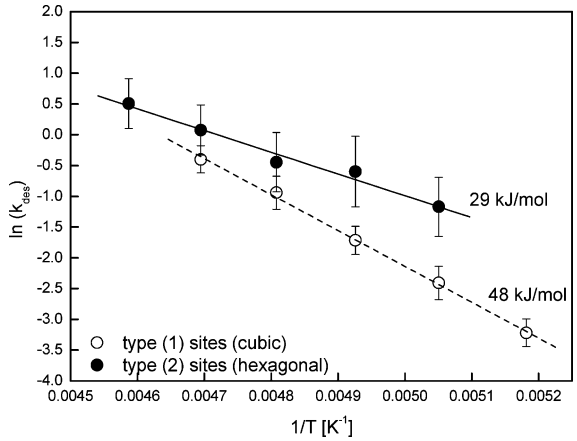

Figure 10. Arrhenius representation of desorption rate coefficients of acetone from cubic (type (1)) and hexagonal (type (2)) surface sites of ice.

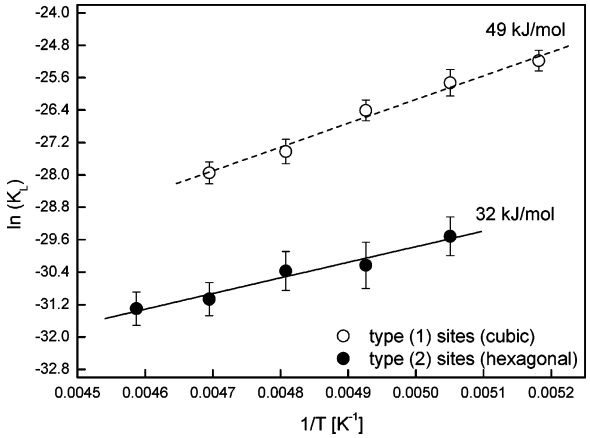

Figure 11. Van t'Hoff representation of the Langmuir constants of acetone on cubic (type (1)) and hexagonal (type (2)) surface sites of ice.

TABLE 2: Summary of Literature Studies for the Adsorption Enthalpies (H_{ads}) and Maximum Number of Surface Sites ($c_{s.max}$) for the Adsorption of Acetone on Ice Surfaces

T range K	ΔH_{ads} kJ mol^{-1}	$c_{s.max}$/ 10^{14} cm^{-2}	technique[k]	ref
0	−31.2[d]		ab initio	64
	−53.4[e]			64
0	−49	2.45	MD	65
50	−46.3	2.45	MD	41
150	−41.8	2.45		41
175	−38.9	1.27		41
average	−43.8[c]		semi	66
193-213	-55 ± 7	-	volumetric	63
198−223	-46 ± 7	2.7 ± 0.7	CWFT	52
190−223	-43.7 ± 7.9	14[g]	CWFT	59
193−223	-48.1 ± 3.1	1.37 ± 0.13	CWFT/Langmuir	58
193−223	-50.3 ± 2.5	1.30 ± 0.18	CWFT/BET	58
203−223	-46 ± 3	< 5%[f]	CWFT	62
205−243	-54.4 ± 7.6[i]	< 5%[f]	chromatography	60
	-56.0 ± 2.8[j]			
198−223	−52[c]	0.1−6%[f]	chromatography	61
130−180	-35 ± 2[a]	100%[f]	TD	72−74
	-40 ± 2[b]	100%[f,h]		
190−220	−49±3	≤ 1[g,h]	CWFT	this work
	−32±6	6[g]		this work

[a] α state. [b] β state. [c] Average value (4 different types of ice). [d] Adsorption on a nondefective surface. [e] Adsorption on a defective surface. [f] Value obtained at this % of the full surface coverage (2.45×10^{14} cm^{-2}). [g] Adsorption capacity depends on ice mass. [h] Annealing reduces adsorption capacity. [i] Ice spheres. [j] Aged snow. [k] CWFT: Coated Wall Flow Tube. TD: Thermal Desorption. MD: Molecular Dynamic.

4. Discussion

Adsorption of acetone on ice has previously been investigated experimentally using a number of different techniques such as CWFT,[1,52,58,59] chromatography,[60−62] Knudsen cells,[13] and volumetric methods.[63] From these studies, kinetic as well as thermodynamic quantities have been derived. In addition, a number of theoretical studies using quantum chemical and molecular dynamical approaches[41,64−66] have been performed. The results obtained with respect to adsorption enthalpies (ΔH_{ads}) and the maximum numbers of adsorption sites ($c_{s,max}$) are summarized in Table 2.

The most important fact to note from this table is the inconsistency/variability of the enthalpy of adsorption, which

differs by almost a factor of 2 between the different studies. Because this quantity reflects the energy change upon interaction of gas-phase acetone with an ice surface, it will depend on a number of parameters (surface coverage, surface morphology and porosity, surface crystallographic phases, and imperfections), none of which can be considered as genuinely invariant between these studies. Moreover, because there is no easy method or technique available by which such variations could be quantified or controlled, the comparison between these results can at best be qualitative.

Nevertheless, one of the experimental parameters that can be reasonably well controlled is surface coverage. As seen from Table 2, most of the experiments performed at low surface coverages ($0.01\% < \theta < 7\%$) yield "high" values of adsorption enthalpies on the order of -50 ± 6 kJ/mol. This is consistent with the value obtained in the present work for a fresh ice surface and a low gas-phase concentration ($<10^{11}$ molecules/cm^3), which is attributed to adsorption on metastable cubic ice. Of the theoretical predictions, agreement with this high value is obtained only if molecular-surface defects are assumed to exist.[64] This is not consistent with our interpretation unless some imperfection of the cubic structure is allowed for. Similarly, high values of ΔH_{ads} were also obtained in a series of chromatographic studies using different ice (polycrystalline, single crystal) and snow samples.[61] Although the experiments were performed on ice samples of different origin and thermal history, preferred adsorption on dislocations and imperfections on the ice surfaces cannot be excluded. Aging effects, however, were not reported.

From more systematic investigations of the dependence of ΔH_{ads} on the extent of surface coverage, Winkler et al.[52] suggest a systematic trend to decreasing values of ΔH_{ads} for increasing coverages even below total surface coverages of 0.07%. This trend could easily be reconciled if coverages were approaching or even exceeding a monolayer. They are difficult to understand, though, if surface coverages are extremely low and in a range where consecutive adsorption events do not influence each other energetically. In contrast to all other experimental techniques, Knudsen cell experiments by Hudson et al.[13] produce a much lower value for the enthalpy of adsorption ($\Delta H°_{ads} = -28 \pm 7$ kJ) this is difficult to explain solely on the basis of surface coverages because Knudsen cells operate, by definition, at very low concentrations and coverages.

In the present investigation, a "low" value for the adsorption enthalpy was obtained for an aged ice surface that has been assigned to be of hexagonal structure. This finding is in agreement with a theoretically predicted result for the adsorption of acetone on a proton-ordered ice surface.[64] Moreover, direct observations of the molecular surface structure under experimental conditions similar to those described by Hudson et al. support the assumption that the value of $\Delta H°_{ads} = -28 \pm 7$ kJ was measured on a ordered hexagonal ice surface. This structure has a "full-bilayer termination", meaning that molecules in the outer layer are bound to the three molecules in the layer below and have just one dangling bond pointing outward, the typical termination of the upper surface of the hexagonal ice structure.[67,68]

Further evidence for the energetic and structural details of gas-phase acetone interacting with an ice surface has been obtained from MD calculations. From investigations of this interaction on proton-ordered ice at 0 K, Picaud et al.[65] found that under these conditions acetone forms an ordered layer on the ice surface with 2 molecules of acetone per surface unit cell of ice. Hence, a monolayer of acetone on ice was found to consist of 2.45×10^{14} molecule cm^{-2}, adsorbed with an energy $\Delta U_{ads} = -49$ kJ/mol. Using the same approach, Picaud and Hoang[41] performed calculations at temperatures between 50 and 150 K, whereupon ΔU_{ads} was found to decrease to -46.3 and -41.8 kJ/mol at 50 and 150 K, respectively. The temperature dependence of the adsorption enthalpy was assigned to the increasing flexibility of the surface molecules with increasing temperature. As opposed to MD calculations, ab initio calculations as performed by Marinelli and Allouche[64] indicate quite different adsorption enthalpies with -53.4 kJ/mol for the adsorption on molecular defects on the ice surface in comparison to -31.2 kJ/mol on proton-ordered hexagonal ice.

In summary, although the majority of experiments performed at low coverages, including our own, produce a high value of the adsorption enthalpy, there is also experimental evidence for lower values. The theoretical results indicate high values only in the presence of surface imperfections, whereas lower values correspond to adsorption on perfectly ordered hexagonal structures. Except for our own work, aging effects have as of yet not been reported. However, we cannot exclude that the effect of aging and the observation of two different enthalpies of adsorption re due to surface imperfections rather than a change between two distinct crystallographic ice phases.

A further inconsistency in the literature data of Table 2 is the maximum surface coverage $c_{s,max}$, for which values between 1.3×10^{14} and 1.4×10^{15} cm^{-2} have been found. From gas phase vapor deposition under our experimental conditions and for a coating time on the order of 1 h, a total number of active surfaces sites on the order of $\sim 1 \times 10^{15}$ cm^{-2} is found in our present experiments. This is in agreement with the ESEM and BET studies of Keyser and Leu[46] and Leu et al. [69] and a previous value from our group.[59] As opposed to these results, all experiments performed on frozen liquid water films produced much lower maximum numbers of active surface sites. This difference is most likely due to surface morphology for which vapor deposition produces a larger roughness and, hence, larger specific surface areas.

A major finding of the present work is the effect of aging of the adsorption capacity. When generating ice films from the condensation of water vapor at low temperatures ($\leq$ 200 K), cubic ice seems to be the preferentially formed ice modification.[45,46] Moreover, there is evidence from a number of other observations that I_c forms easily at lower temperatures. For instance, supercooled water preferentially freezes to cubic ice at sufficiently cold temperatures.[70] Clusters of 4000−6000 water molecules have been shown to nucleate exclusively to I_c when cooled by evaporation to 200 K.[70] Rapid quenching of 3 μm droplets on a cryoplate led to I_c at 190 K but to I_h at 200 K.[71] However, cubic ice is a metastable phase that tends to transform into the thermodynamically stable hexagonal phase on a time scale of several 10 min at temperatures around 200 K.[44,46−49]

Different adsorption behavior of acetone on ice surfaces depending on the thermal history of the ice has previously been observed in thermal desorption (TPD) experiments under ultrahigh vacuum (UHV) conditions.[72−74] From the preparation of thin ice films (10−100 monolayers) by condensation of water vapor onto the cold (90−130 K) metal substrate, two desorption peaks of acetone at 140 and 157 K, designated α- and β-acetone, respectively, were observed during TPD. Assuming first-order desorption kinetics and frequency factors of 10^{13} s^{-1} [75], the corresponding activation energies were approximately 35 and 40 kJ mol^{-1}, respectively. Annealing of the ice surface lead to irreversible change of the desorption behavior for which only the lower temperature state (α-acetone) was observed, very

much in agreement with the present findings on the kinetics of acetone adsorption under surface aging conditions. These authors, however, differ from us in assigning the higher temperature desorbing β-acetone to correspond to an adsorption on amorphous ice rather than cubic ice. Although the existence of a thermally metastable cubic ice phase has been suggested from electron microscopy and electron diffraction studies,[48] other observations favor the existence of amorphous ice at temperatures below 140 K.[76] IR-spectroscopic studies performed by Schaff and Roberts[72−74] also indicated differences in the surface chemical structure of the two ice phases. Whereas for the α-adsorption state no specific hydrogen bonding is detectable and the adsorption is referred to as physisorption, adsorption in the β-state is via free and dangling OH bonds.

Experiments reported by Chaix et al.[47] for the adsorption of D_2O on ice suggest that both the method of preparation and the thermal history of the ice sample influence the morphology and the microstructure of the sample and, hence, its adsorption kinetics. For instance, it was found that the annealing of cubic ice, prepared by condensing water vapor at 140 K, reduces the γ value for adsorption of D_2O irreversibly by a factor of 2. It is also worthy of note that in our work, we also observe a significant difference in γ values for fresh and aged ice with the higher value being measured for cubic ice. Although this difference may hint toward a contribution to adsorption at fresh ice by surface imperfections, similar differences have also been reported for the adsorption of H_2O on ice surfaces.[89]

As discussed in the above sections of this work, we suggest that the observed aging behavior of our ice films, as noted at lower temperatures, is caused by a change of the crystallographic phase of available surface sites, namely from cubic to hexagonal. Any other explanation for the observed aging effect, i.e., a change of surface topography or morphology, the presence of molecular surface defects, as well as embossed or engraved microstructures, is left unconsidered. Of these, the lifetime of molecular surface defects should be in the order of milliseconds, much shorter than the time scale of aging as observed in our work. This is because of the high dynamics of the surface bilayer structure[42] and the fast adoption/desorption kinetics at 198 K.[47] The presence of microstructures, on the other hand, is not expected to change as a result of the dynamical behavior of the surfaces structure but to sustain on the time scale of hours. Therefore, we cannot, in principle, exclude changes of the surface microstructures to be responsible for our observed aging effects. Nevertheless, our observations do not contradict recent observations reported in the literature on observed crystallographic changes of ice surfaces.[44,77]

One of the more significant and characteristic observations of cubic to hexagonal ice conversions that have been reported is the rate of change and its temperature dependence.[44,78] Measurements in the temperature range 160−220 K indicate activation energies on the order of 34 kJ/mol and characteristic times between 10^4 and 10 min.[44] This is very much consistent with the findings of the present work and, therefore, lends independent support for our conclusions. Formation of metastable cubic ice and its subsequent thermal conversion into stable hexagonal ice is supposed to occur because the rate of surface reconstruction to a structure of lower potential energy is slow in comparison to the rate of condensation. In addition, cubic ice may have a more energetic and reactive surface with highly irregular surface structure and a substantial fraction of incompletely coordinated surface water molecules**.** Indeed, computer simulation suggests significant modification of the ice surface structure with respect to the cubic crystalline interior, toward loss of lateral order at 200 K.[79] During annealing, a transition of the ice structure from cubic to hexagonal is expected.[44,77]

In addition, the observed decrease of the adsorption capacity is consistent with the assumed shrinking of the size of cubic ice crystals, which is correlated with the mass transfer between I_c and I_h.[77] Because both modifications share a common vapor phase, the differences in the vapor pressure, as estimated from measurements of the free enthalpy of transformation of I_c to I_h at around 200 K ($\Delta G \approx 50-160$ J/mol[71,80−82]), leads to a continuous decrease of the surface area of the cubic crystals. A more detailed discussion of the conversion I_c to I_h depending on temperature and the size of the cubic crystals in comparison with the model of Murphy[77] is in preparation.[57]

5. Summary and Conclusions

We have investigated acetone adsorption on ice surfaces and have determined kinetic and thermodynamic constants associated with this uptake. Moreover, our studies present evidence that these constants are influenced by an aging effect of the surface leading to a reduction of the adsorptive capacity. This change can, in principle, be caused by a number of reasons, including crystallographic changes or the presence of surface site imperfection on both the molecular and the microstructure level. Although we do not have direct proof, we still argue that this aging effect is associated with a change of the crystallographic phase of our ice films from initially metastable cubic to finally hexagonal.

The results of our study have not unravelled all of the discrepancies/inconsistencies in the set of available literature studies on the adsorption behavior of acetone on ice surfaces. These discrepancies are thought to be jointly caused by insufficient experimental control over parameters such as surface morphology, total available surface area, number of active adsorption sites, crystallographic phases and their imperfections, etc. Therefore, it is suggested that further clarification on kinetic and thermodynamic quantities for gas-phase adsorption on highly dynamic surfaces such as ice is accompanied by improved surface characterizations using morphology (i.e., ESEM) or chemical (i.e., DRIFTS) sensitive techniques.

Finally it needs to be pointed out that the present finding of phase-related adsorption properties of acetone on ice might also be of relevance to the atmospheric environment. An important mechanism for ice cloud formation is homogeneous nucleation of ice in aqueous droplets. This process is generally assumed to produce hexagonal ice.[83,84] However, there are some reports that the metastable cubic crystalline phase of ice may also form in the Earth's atmosphere.[77,85,86] A much more direct observation of I_c was made in Antarctic polar stratospheric clouds, where about 25% of the ice crystals had clearly cubic morphology.[87] Moreover, recent experiments confirm that the formation of cubic ice is dominant when droplets freeze at temperatures below 190 K, which is in the temperature range relevant for polar stratospheric clouds and clouds in the tropical tropopause region.[88] If there were a significant fraction of cubic ice in some cold clouds, this could increase their water vapor pressure and modify their microphysics, ice particle size distributions, and heterogeneous chemistry.

Acknowledgment. We gratefully acknowledge financial support of this work by the European Commission via the CUT-ICE project (EVK2-CT1999) as well as by Flughafen−Stiftung Frankfurt am Main. We also thank one of the referees for very helpful discussion and comments.

References and Notes

(1) Behr, P.; Terziyski, A.; Zellner, R. *Z. Phys. Chem.* **2004**, *218*, 1307−1327.

(2) Farman, J. C.; Gardiner, B. J.; Chanklin, G. G. *Nature* **1985**, *315*, 207−210.
(3) Lelieveld, J.; Bregman, A.; Scheeren, H. A.; Strom, J.; Carslaw, K. S.; Fischer, H.; Siegmund, P. C.; Arnold, F. *J. Geophys. Res., Atmos.* **1999**, *104*, 8201−8213.
(4) Solomon, S. *Rev. Geophys.* **1999**, *37*, 275−316.
(5) Crutzen, P. J.; Lelieveld, J. *Annu. Rev. Earth Planet. Sci.* **2001**, *29*, 17−45.
(6) Lorenzen-Schmidt, H.; Wessel, S.; Unold, W.; Solberg, S.; Gernandt, H.; Stordal, F.; Platt, U. *Tellus, Ser. B* **1998**, *50*, 416−429.
(7) Wessel, S.; Aoki, S.; Winkler, P.; Weller, R.; Herber, A.; Gernandt, H.; Schrems, O. *Tellus, Ser. B* **1998**, *50*, 34−50.
(8) Platt, U.; Honninger, G. *Chemosphere* **2003**, *52*, 325−338.
(9) Zellner R. Chemistry of the Stratosphere. In *Global Aspects of Atmospheric Chemistry, Topics in Physical Chemistry*; Baumgärtel, H., Grünbein, W., Hensel, F., Zellner R., Eds.; Steinkopff/Springer: Darmstadt 1999; pp 181−247.
(10) Dankwerts, P. V. *Trans. Faraday Soc.* **1951**, *47*, 1014−1023.
(11) Kolb, C. E.; Worsnop, D. R.; Zahniser, M. S.; Davidovits, P.; Keyser, L. F.; Leu, M. T.; Molina, M. J.; Hanson, D. R.; Ravishankara, A. R.; Williams, L. R.; Tolbert, M. A. Laboratory Studies of Atmospheric Heterogeneous Chemistry. In *Progress and Problems in Atmospheric Chemistry*; Barker J. R., Ed.; Advanced Series in Physical Chemistry 3; World Scientific: River Edge, NJ, 1995; p 771.
(12) Zondlo, M. A.; Barone, S. B.; Tolbert, M. A. *J. Phys. Chem. A* **1998**, *102*, 5735−5748.
(13) Hudson, P. K.; Zondlo, M. A.; Tolbert, M. A. *J. Phys. Chem. A* **2002**, *106*, 2882−2888.
(14) Nathanson, G. M.; Davidovits, P.; Worsnop, D. R.; Kolb, C. E. *J. Phys. Chem.* **1996**, *100*, 13007−13020.
(15) Rudich, Y.; Talukdar, R. K.; Imamura, T.; Fox, R. W.; Ravishankara, A. R. *Chem. Phys. Lett.* **1996**, *261*, 467−473.
(16) Behr, P.; Morris, J. R.; Antman, M. D.; Ringeisen, B. R.; Splan, J. R.; Nathanson, G. M. *Geophys. Res. Lett.* **2001**, *28*, 1961−1964.
(17) Wagner, S.; Röth, E. P.; Zellner R. **2006**, to be published.
(18) Marx, D.; Hutter, J. Ab Initio Molecular Dynamics: Theory and Implementation. In *Modern Methods and Algorithms of Quantum Chemistry: Proceedings*; Grotendorst, J., Ed.; Publications of the John von Neumann Institute for Computing (NIC), NIC Series; NIC: Juelich, Germany, 2000; Vol. 1.
(19) Galashev, A. E.; Pozharskaya, G. L.; Chukanov, V. N. *J. Struct. Chem.* **2002**, *43*, 458−466.
(20) Toon, O. B.; Turco, R. P.; Jordan J.; Goodman, J.; Ferry, G. *J. Geophys. Res.* **1989**, *94*, 11359−11380.
(21) Fahey, D. W.; Kelly, K. K.; Ferry, G. V.; Poole, L. R.; Wilson, J. C.; Murphy, D. M.; Loewenstein, R.; Chan, K. R. *J. Geophys. Res.* **1989**, *94*, 11299−11315.
(22) Larsen, N.; Svendsen, S. H.; Knudsen, B. M.; Voigt, C.; Weisser, C.; Kohlmann, A.; Schreiner, J.; Mauersberger, K.; Deshler, T.; Kroger, C.; Rosen, J. M.; Kjome, N. T.; Adriani, A.; Cairo, F.; Di Donfrancesco, G.; Ovarlez, J.; Ovarlez, H.; Dornbrack, A.; Birner, T. *J. Geophys. Res., Atmos.* **2002**, *107*, Art. No. 8301.
(23) Pruppacher, H. R.; Klett, J. D. *Atmospheric and Oceanographic Sciences Library*, Vol 18; Kluwer Academic Pub.: Boston, 1996.
(24) Seinfeld, J. H.; Pandis, S. N. *Atmosperic Chemistry and Physics: From Air Pollution to Climate Change*; John Wiley & Sons: U.S.A., 1998.
(25) Gleitsmann, G.; Zellner, R. *Atmos. Environ.* **1998**, *32*, 3079−3087.
(26) Gierens, K. *Atmos. Chem. Phys.* **2003**, *3*, 437−446.
(27) Blyth, A. M.; Christian, H. J.; Driscoll, K.; Gadian, A. M.; Latham, J. *Atmos. Res.* **2001**, *59*, 217−229.
(28) Dash, J. G.; Wettlaufer, J. S. *Can. J. Phys.* **2003**, *81*, 201−207.
(29) Abbatt, J. P. D. *Chem. Rev.* **2003**, *103*, 4783−4800.
(30) Arnold, F.; Schneider, J.; Gollinger, K.; Schlager, H.; Schulte, P.; Hagen, D. E.; Whitefield, P. D.; Vanvelthoven, P. *Geophys. Res. Lett.* **1997**, *24*, 57−60.
(31) Singh, H.; Chen, Y.; Tabazadeh, A.; Fukui, Y.; Bey, I.; Yantosca, R.; Jacob, D.; Arnold, F.; Wohlfrom, K.; Atlas, E.; Flocke, F.; Blake, D.; Blake, N.; Heikes, B.; Snow, J.; Talbot, R.; Gregory, G.; Sachse, G.; Vay, S.; Kondo, Y. *J. Geophys. Res., Atmos.* **2000**, *105*, 3795−3805.
(32) Singh, H. B.; Kanakidou, M.; Crutzen, P. J.; Jacob, D. J. *Nature* **1995**, *378*, 50−54.
(33) Mckeen, S. A.; Gierczak, T.; Burkholder, J. B.; Wennberg, P. O.; Hanisco, T. F.; Keim, E. R.; Gao, R. S.; Liu, S. C.; Ravishankara, A. R.; Fahey, D. W. *Geophys. Res. Lett.* **1997**, *24*, 3177−3180.
(34) Jaegle, L.; Jacob, D. J.; Brune, W. H.; Wennberg, P. O. *Atmos. Environ.* **2001**, *35*, 469.
(35) Howard, C. J. *J. Phys. Chem*, **1979**, *83*, 3−9.
(36) Bedjanian, Y.; Poulet, G. *Chem. Rev.* **2003**, *103*, 4639−4655.
(37) Klassen, J. K.; Fiehrer, K. M.; Nathanson, G. M. *J. Phys. Chem. B* **1997**, *101*, 9098−9106.
(38) Isakson, M. J.; Sitz, G. O. *J. Phys. Chem. A* **1999**, *103*, 2044−2049.
(39) Morris, J. R.; Behr, P.; Antman, M. D.; Ringeisen, B. R.; Splan, J.; Nathanson, G. M. *J. Phys. Chem. A* **2000**, *104*, 6738−6751.
(40) Ertl, G. *Science* **1991**, *254*, 1750−1755.
(41) Picaud, S.; Hoang, P. N. M. *J. Chem. Phys.* **2000**, *112*, 9898−9908.
(42) Girardet, C.; Toubin, C. *Surf. Sci. Rep.* **2001**, *44*, 163−238.
(43) Petrenko, V. F.; Whitworth, R. W. *Physics of Ice*; Oxford University Press: New York, 1999.
(44) Dowell, L. G.; Rinfret, A. P. *Nature* **1960**, *188*, 1144−1148.
(45) Hobbs, P. V. *Ice Physics*; Clarendon Press: Oxford, 1974; pp 44−60.
(46) Keyser, L. F.; Leu, M. T. *Microsc. Res. Technol.* **1993**, *25*, 434−438.
(47) Chaix, L.; Van Den Bergh, H.; Rossi, M. J. *J. Phys. Chem. A* **1998**, *102*, 10300−10309.
(48) Kumai, M. *J. Glaciol.* **1968**, *7*.
(49) Davy, J. G.; Somorjai, G. A. *J. Chem. Phys.* **1971**, *55*, 3624−3636.
(50) Hynes, R. G.; Fernandez, M. A.; Cox, R. A. *J. Geophys. Res., Atmos.* **2002**, *107*.
(51) Sokolov, O.; Abbatt, J. P. D. *J. Phys. Chem. A* **2002**, *106*, 775−782.
(52) Winkler, A. K.; Holmes, N. S.; Crowley, J. N. *Phys. Chem. Chem. Phys.* **2002**, *4*, 5270−5275.
(53) Journet, E.; Le Calve, S.; Mirabel, P. *J. Phys. Chem. B* **2005**, *109*, 14112−14117.
(54) Cox, R. A.; Fernandez; M. A.; Symington, A.; Ullerstam, M.; Abbatt, J. P. D. *Phys. Chem. Chem. Phys.* **2005**, *7*, 3434−3442.
(55) Speedy, R. J.; Debenedetti, P. G.; Smith, R. S.; Huang, C.; Kay, B. D. *J. Chem. Phys.* **1996**, *105*, 240−244.
(56) Delval, C.; Fluckiger, B.; Rossi, M. J. *Atmos. Chem. Phys*, **2003**, *3*, 1131−1145.
(57) Behr, P.; Terziyski, A.; Zellner, R. **2006**, to be published.
(58) Peybernes, N.; Marchand, C.; Le Calve, S.; Mirabel, P. *Phys. Chem. Chem. Phys.* **2004**, *6*, 1277−1284.
(59) Behr, P.; Scharfenort, U.; Terziyski, A.; Demiral, K.; Zellner, R. *Int. Symp. Combust. Atmos. Pollut.* **2003**, 575−578.
(60) Guimbaud, C.; Bartels-Rausch, T.; Ammann, M. *Int. J. Mass Spectrom.* **2003**, *226*, 279−290.
(61) Bartels-Rausch, T.; Guimbaud, C.; Gaggeler, H. W.; Ammann, M. *Geophys. Res. Lett.* **2004**, *31*.
(62) Bartels-Rausch, T.; Huthwelker, T.; Gaggeler, H. W.; Ammann, M. *J. Phys. Chem. A* **2005**, *109*, 4531−4539.
(63) Domine, F.; Rey-Hanot, L. *Geophys. Res. Lett.* **2002**, *29*.
(64) Marinelli, F.; Allouche, A. *Chem. Phys.* **2001**, *272*, 137−147.
(65) Picaud, S.; Toubin, C.; Girardet, C. *Surf. Sci.* **2000**, *454*, 178−182.
(66) Girardet, C.; Toubin, C. *Surf. Sci. Rep*, **2001**, *44*, 159−238.
(67) Braun, J.; Glebov, A.; Graham, A. P.; Menzel, A.; Toennies J. P. *Phys. Rev. Lett.* **1998**, *80*, 2638−2641.
(68) Materer, N.; Starke, U.; Barbieri, A.; Vanhove, M. A.; Somorjai, G. A.; Kroes, G. J.; Minot, C. *Surf. Sci.* **1997**, *381*, 190−210.
(69) Leu, M. T.; Keyser, L. F.; Timonen, R. S. *J. Phys. Chem. B* **1997**, *101*, 6259−6262.
(70) Huang, J. F.; Bartell, L. S. *J. Phys. Chem.* **1995**, *99*, 3924−3931.
(71) Mayer, E.; Hallbrucker, A. *Nature* **1987**, *325*, 601−602.
(72) Schaff, J. E.; Roberts, J. T. *Langmuir* **1998**, *14*, 1478−1486.
(73) Schaff, J. E.; Roberts, J. T. *J. Phys. Chem.* **1996**, *100*, 14151−14160.
(74) Schaff, J. E.; Roberts, J. T. *J. Phys. Chem.* **1994**, *98*, 6900−6902.
(75) Yates, J. T. J. *Methods Exp. Phys.* **1985**, *22*, 425−465.
(76) Burton, E. F.; Oliver, W. F. *Proc. R. Soc. London, Ser. A* **1935**, *153*, 166−172.
(77) Murphy, D. M. *Geophys. Res. Lett.* **2003**, *30*, 2230.
(78) Bertie, J. E.; Calvert, L. D.; Whalley, E. *J. Chem. Phys*, **1963**, *38*, 840−846.
(79) Devlin, J. P.; Buch, V. *J. Phys. Chem.* **1995**, *99*, 16534−16548.
(80) Handa, Y. P.; Klug, D. D.; Whalley, E. *J. Phys. Chem.* **1986,** *84*, 7009−7010.
(81) McMillan, J. A.; Los, S. C. *Nature* **1965**, *206*, 806−807.
(82) Sugisaki, M.; Suga, H.; Seki, S. *Bull. Chem. Soc. Jpn.* **1968**, *41*, 2591−2599.
(83) Young, K. C. *Mircophysical Processes in Clouds*; Oxford University Press: New York, 1993.
(84) Pruppacher, H. R.; Klett, J. D. *Microphysics of Clouds and Precipitation*; Kluwer: Dordrecht, 1997.
(85) Whalley, E. *Science* **1981**, *211*, 389−390.
(86) Riikonen, M.; Sillanpaa, M.; Virta, L.; Sullivan, D.; Moilanen, J.; Luukkonen, I. *Appl. Opt.* **2000**, *39*, 6080−6085.
(87) Goodman, J.; Toon, O. B.; Pueschel, R. F.; Snetsinger, K. G.; Verma, S. *J. Geophys. Res.* **1989**, *94*, 16449−16457.
(88) Murray, B. J.; Knopf, D. A.; Bertram, A. K. *Nature* **2005**, *434*, 202−205.
(89) Pratte, P.; van den Berg, H.; Rossi, M. J. *J. Phys. Chem.* A **2006**, *110*, 3042−3058.